Available online at www.sciencedirect.com
SCIENCE DIRECT®
Journal of Solid State Chemistry 175 (2003) 63–71
JOURNAL OF SOLID STATE CHEMISTRY
http://elsevier.com/locate/jssc

Comparison of one-, two-, and three-dimensional iron phosphates containing ethylenediamine

Yanning Song, Peter Y. Zavalij, Natasha A. Chernova, Masatsugu Suzuki, and M. Stanley Whittingham*

Department of Chemistry and Institute for Materials Research, State University of New York at Binghamton, Binghamton, NY, 13902-6000, USA

Received 19 November 2002; received in revised form 1 March 2003; accepted 7 March 2003

Abstract

A new two-dimensional (2d) iron phosphate, $(C_2N_2H_{10})Fe_2O(PO_4)_2$, has been synthesized under hydrothermal conditions in the system of $FeCl_3$–H_3PO_4–$C_2N_2H_8$–H_2O. The crystal data is: space group $P2_1/c$, $a = 10.670(1)$ Å, $b = 10.897(1)$ Å, $c = 9.918(1)$ Å, $\beta = 105.632(1)^\circ$, $Z = 4$. The layered structure consists of double sheet layers, of composition $Fe_2O(PO_4)_2$, built from FeO_5 trigonal bipyramids and PO_4 tetrahedra. The amine holds the layers together via H-bonding. The study of the magnetic properties reveals two magnetic transitions at 160 and 30 K with spin-glass-like behavior below 160 K. By varying the hydrothermal conditions, three other iron phosphates were synthesized: the one-dimensional (1d) $(C_2N_2H_{10})Fe(HPO_4)_2(OH)\cdot H_2O$, the 2d $(C_2N_2H_{10})Fe_2(PO_4)_2(OH)_2$, and the three-dimensional (3d) $(C_2N_2H_{10})_2Fe_4O(PO_4)_4\cdot H_2O$. The 1d compound can be used as the starting reagent in the synthesis of both the 2d compound and the 3d lipscombite $Fe_3(PO_4)_2(OH)_2$ due to the similar building blocks in their structures. In the 3d phosphate $(C_2N_2H_{10})_2Fe_4O(PO_4)_4\cdot H_2O$, manganese can substitute for half of the iron atoms. Magnetic study shows ordering transitions at about 30 K, however, manganese substitution depresses the magnetic ordering temperature.

1. Introduction

As more and more open-framework inorganic materials are synthesized for possible application in the field of heterogeneous catalysis, separation and ion exchange processes [1], the opportunity arises to study other properties, such as magnetic susceptibility as a function of structure type. One such class of potentially interesting materials are the transition metal phosphates. In nature, iron phosphate minerals have a rich crystal chemistry and are viewed as one of the most perplexing classes of minerals [2]. Recently, at least four different iron phosphate phases have been identified [3]. In the synthesis of open-framework structures, the hydrothermal method is widely employed with the help of structure-directing agents. Diamines, with their high charge distribution, have long been used as templates in the hydrothermal synthesis of molybdenum phosphates [4,5], indium phosphates [6] and vanadium phosphates [7]. In the last decade many new iron phosphate compounds have also been synthesized [8–25]. These compounds have one-dimensional (1d) chain [8–12], two-dimensional (2d) layered [13–19] and three-dimensional (3d) [10,20–25] open-framework structures. The synthesis and structures of these compounds have been reviewed by Lii et al. [26]. A great deal of effort has also been focused on understanding the mechanism of crystallization in the black-box of the hydrothermal system. It is believed that basic building units are involved in the formation of phosphates with different dimensionalities [27]. In situ X-ray diffraction and NMR studies of gallium phosphates [28–30] and more recently zinc phosphates [31–34] under hydrothermal conditions have revealed the transformation of the precursor units to the final structure.

We report here the synthesis, crystal structure and magnetic properties of a new 2d iron phosphate, and compare it to other iron phosphates with related structures to help understand their hydrothermal synthesis and physical properties.

*Corresponding author. Fax: +1-607-777-4623.
E-mail address: stanwhit@binghamton.edu (M.S. Whittingham).

0022-4596/03/$ - see front matter © 2003 Elsevier Inc. All rights reserved.
doi:10.1016/S0022-4596(03)00144-0

2. Experimental section

2.1. Synthesis

The syntheses of the compounds were carried out by hydrothermal reaction. Different amount of $FeCl_3 \cdot 6H_2O$ (J.T. Baker), $MnCl_2 \cdot 4H_2O$ (Fisher), $H_2NCH_2CH_2NH_2$ (Aldrich, abbreviated as en), H_3PO_4 (Fisher) and H_2O were placed in 125 mL Teflon-lined Parr™ autoclaves for hydrothermal synthesis. The pH of the solution before and after hydrothermal reaction was measured. The detailed reaction conditions are outlined in Table 1. By varying the synthesis conditions, several different iron phosphates can be synthesized as pure phase rather than as mixtures. The products include orange plates of the novel compound $(enH_2)Fe_2O(PO_4)_2$ (2d-*A*), green needles of $(enH_2)Fe(HPO_4)_2(OH) \cdot H_2O$ (1d) [12], yellow plates of $(enH_2)Fe_2(PO_4)_2(OH)_2$ (2d-*B*) [16], black cubes of $(enH_2)_2Fe_4O(PO_4)_4 \cdot H_2O$ (3d-Fe) [20,24] and black powders of lipscombite $Fe_3(PO_4)_2(OH)_2$ (Lip) [35]. When manganese was substituted for iron in the 3d-Fe compound, black cubic crystals (3d-Mn) were obtained. The molar ratio of Fe/Mn in 3d-Mn, determined by direct current plasma atomic emission spectroscopy (DCP-AES, ARL SS-7 DCP), is 1.07:1 close to the expected 1:1 ratio.

2.2. Structure determination

The products were identified by powder or single crystal X-ray diffraction. Powder diffraction patterns were recorded on a Scintag XDS2000 $\theta - \theta$ powder diffractometer equipped with a Ge(Li) solid state detector (Cu$K\alpha$ radiation). The single crystal data was collected on a Bruker Smart Apex diffractometer at room temperature (Mo$K\alpha$ radiation, graphite monochromator); the crystals were carefully selected under a microscope and glued to a thin glass fiber with super glue adhesive. Full reciprocal sphere was scanned and integral intensities were corrected for absorption effect using SADBAS software. Crystal structures were solved by direct methods using SHELXS and refined using SHELXL97 software [36]. The crystallographic data and pertinent experimental details are presented in Table 2; the atomic coordinates and displacement parameters are listed in Table 3, and selected bond length and angles in Table 4.

2.3. Thermal gravimetric analysis (TGA)

TGA was performed on a Perkin–Elmer TGA in oxygen at a heating rate of $5^\circ C\,min^{-1}$. The products after TGA were identified by powder X-ray diffraction.

2.4. Fourier transform infrared (FTIR)

FTIR was performed on a Bruker EQUINOX 55 instrument using KBr pellets.

Table 2
Crystallographic data of $(C_2N_2H_{10})Fe_2O(PO_4)_2$

Molecular formula	$C_2H_{10}Fe_2N_2O_9P_2$
Formula weight	$379.76\,g\,mol^{-1}$
Color	Orange
Size	$0.005 \times 0.14 \times 0.20\,mm^3$
Crystal system	Monoclinic
Space group	$P2_1/c$
a	10.6696(9) Å
b	9.8969(8) Å
c	9.9182(8) Å
β	105.632(1)°
V	1008.6(1) $Å^3$
Z	4
Temperature, T	20°C
Wavelength, λ (Mo$K\alpha$)	0.71073 Å
Density, ρ_{calc}	$2.501\,g\,cm^{-3}$
Linear absorption, μ	$32.37\,cm^{-1}$
Minimal transmission, T_{min}	0.400
Maximal transmission, T_{max}	0.984
Measured reflections	4647
Unique reflections	1792
Observed reflections ($I > 2\sigma$)	1324
Parameters	156
R_{eqiv}	0.0621
R_w	0.0657
$R_F(I > 2\sigma)$	0.0397

Table 1
Synthesis of iron phosphates

$FeCl_3$ (mol)	H_3PO_4 (mol)	en (mL)	H_2O (mL)	Initial pH	Final pH	Temp. (°C)	Time (h)	Product
0.005	0.04	2.5	35	6.31	6.49	150	2.5	1d*
0.005	0.04	2.5	35	6.35	6.43	150	10	1d + lip
0.005	0.02	1.3	35	6.32	6.20	170	70	2d-*A* + 2d-*B* + lip
0.01	0.04	4.5	35	8.16	8.35	170	3	2d-*B*
0.005	0.02	2.0	35	8.20	8.62	170	96	2d-*A* + 2d-*B* + 3d-Fe + lip**
0.02	0.02	0.7	35	0.55	0.50	170	70	Monoclinic $FePO_4 \cdot 2H_2O$

*0.305 g 1d + 0.002 mol H_3PO_4 + 20 mL H_2O, adjusted pH to 9.66, after 15 h at 170°C, pH turned to 9.23 with product of pure 2d-*B*; 0.2 g 1d + 20 mL H_2O, pH changed from 6.59 to 5.94 after 40 h at 200°C with product of lip.

**3d-Mn was synthesized the same as 3d-Fe except that the reactants are 0.001 mol $FeCl_3$, 0.001 mol $MnCl_2$, 0.004 mol H_3PO_4. The initial and final pH is 9.30 and 10.02, respectively.

Table 3
Atomic coordinates and equivalent atomic displacement parameters for $(C_2N_2H_{10})Fe_2O(PO_4)_2$

Atom	x	y	z	U_{eq} (Å^2)
Fe1	0.64232(7)	0.15017(6)	0.78006(7)	0.0110(2)
Fe2	0.37884(7)	0.07189(6)	0.48498(7)	0.0108(2)
O1	0.5431(3)	0.0628(3)	0.6139(3)	0.0114(8)
P1	0.3857(1)	0.3311(1)	0.6898(1)	0.0122(3)
O2	0.5332(3)	0.3105(3)	0.7364(3)	0.0159(8)
O3	0.3186(3)	0.2250(3)	0.5824(3)	0.0152(8)
O4	0.3546(3)	0.4723(3)	0.6262(3)	0.0180(9)
O5	0.3300(3)	0.3139(3)	0.8176(3)	0.0177(9)
P2	0.8036(1)	0.1828(1)	0.5600(1)	0.0119(3)
O6	0.7902(3)	0.1858(3)	0.7139(3)	0.0129(8)
O7	0.7620(3)	0.0409(3)	0.4982(3)	0.0166(9)
O8	0.7128(3)	0.2899(3)	0.4750(3)	0.0185(9)
O9	0.9437(3)	0.2116(3)	0.5676(4)	0.0180(9)
N1	0.0684(4)	0.2898(4)	0.3728(4)	0.024(1)
C1	0.0731(6)	0.4397(5)	0.3670(6)	0.023(1)
C2	0.1490(6)	0.4883(5)	0.2674(6)	0.022(1)
N2	0.2918(4)	0.4800(4)	0.3288(4)	0.023(1)

Table 4
Selected bond distances (Å), bond and torsion angles (deg) for $(C_2N_2H_{10})Fe_2O(PO_4)_2$

Fe1–O6	1.898(3)	O6–Fe1–O2	105.96(14)
Fe1–O1	1.909(3)	O1–Fe1–O8^{i}	163.94(14)
Fe1–O2	1.947(3)	O6–Fe1–O4^{ii}	114.58(14)
Fe1–O8^{i}	1.968(3)	O2–Fe1–O4^{ii}	139.43(15)
Fe1–O4^{ii}	1.987(3)	O1–Fe2–O7^{iii}	121.61(14)
Fe2–O1	1.873(3)	O1–Fe2–O5^{iv}	126.34(14)
Fe2–O7^{iii}	1.915(3)	^{iii}O7–Fe2–O5^{iv}	112.00(15)
Fe2–O5^{iv}	1.959(3)	^{iii}O1–Fe2–O3	172.31(14)
Fe2–O1^{iii}	1.969(3)	N1–C1–C2–N2	−78.4(5)
Fe2–O3	1.995(3)		

Symmetry codes: (i) $x, 1/2-y, 1/2+z$; (ii) $1-x, y-1/2, 3/2-z$; (iii) $1-x, -y, 1-z$; (iv) $x, 1/2-y, z-1/2$.

2.5. Magnetic measurements

The temperature-dependent dc magnetic susceptibility was measured using a Quantum Design MPMS XL SQUID Magnetometer in a magnetic field of 1000 Oe over a temperature range of 2–298 K at 2 K intervals. After holding in a zero field at 298 K for 20 min, samples were cooled to 2 K at zero field. The zero-field-cooled (ZFC) susceptibilities were measured at 100 Oe over a temperature range from 2 K to different temperatures (T_1) depending on the transition temperature observed in the dc susceptibility measurement. Then samples were annealed at 298 K for 20 min with a field of 100 Oe and subsequently cooled to T_1 in a 100 Oe field. Field cooled (FC) susceptibilities were measured from T_1 to 2 K in the field of 100 Oe.

3. Results and discussion

3.1. Synthesis and initial characterization

A number of factors affect the synthesis of the compounds, as shown in Table 1. The 1d chain structure can be easily obtained with high purity even at 150°C for 3 h. Increasing the concentration of phosphoric acid (low pH) favors the formation of the 1d chain compound, while increasing the concentration of the amine (high pH) helps the formation of the high-dimensional framework. Interestingly, when the 1d chain product was placed into a mixture of amine and phosphate under hydrothermal conditions of 170°C for 15 h with pH around 9, it was converted to the 2d-*B* compound. The similarity in the structural building blocks of these compounds suggests that the higher dimensional structure might be built up from the lower dimensional structure. When placed in water for 40 h at 200°C, the 1d compound loses the amine and turns into lipscombite $Fe_3(PO_4)_2(OH)_2$ (Lip). At low pH values, the amine is unable to be incorporated into the iron phosphate structure, yielding monoclinic $FePO_4 \cdot 2H_2O$ [3].

Thermal analysis shows that the decomposition of the amine in all these materials occurs in two steps (Fig. 1). This is typical for the iron phosphate materials with ethylene diamine as template [37]. The experimental weight loss is in good agreement with the calculated value, as shown in Table 5.

FTIR shows P–O vibration peaks at around 800–1200 cm^{-1}, sharp C–N vibration peaks at around 1500 cm^{-1} and N–H vibration peaks at around 3500 cm^{-1} in all the compounds, as shown in Fig. 2. However, the O–H vibration peaks at around 3200 cm^{-1} are only present in the 1d and 2d-*B* materials. This agrees well with their formulae. The manganese

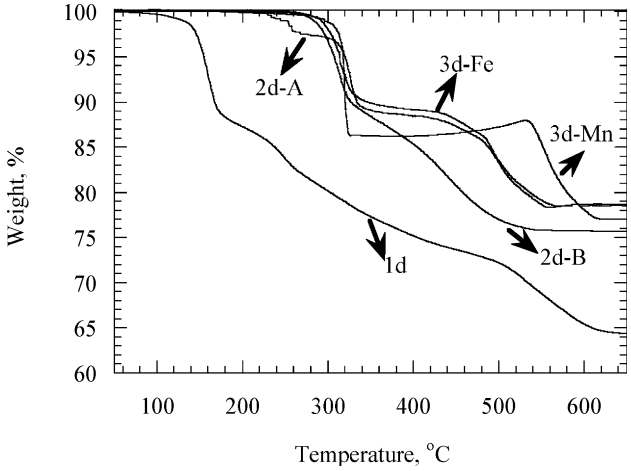

Fig. 1. TGA of iron phosphate materials; 5°C min^{-1} in air.

Table 5
TGA of iron phosphate materials

	Experimental weight loss (%)	Theoretical weight loss (%)	Product after TGA
1d	35.73	35.70*	Amorphous
2d-*A*	21.48	20.57	$FePO_4$
2d-*B*	24.35	24.17	$FePO_4$
3d-Fe	21.35	20.78	$FePO_4$
3d-Mn	23.00	22.94	$FePO_4 + Mn_2P_2O_7$

*The value is calculated based on the product as mixture of $FePO_4$ and P_2O_5.

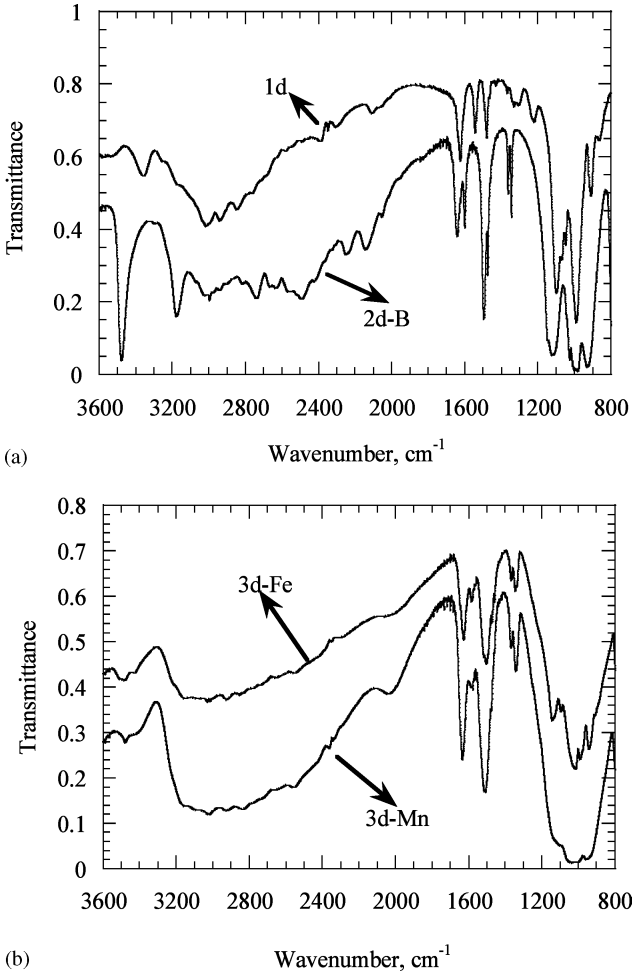

Fig. 2. FTIR of (a) 1d and 2d-*B*, (b) 3d-Fe and 3d-Mn materials.

substitution does not change the FTIR spectra as shown in Fig. 2b.

3.2. Crystal structure of $(enH_2)Fe_2O(PO_4)_2$

The asymmetric unit of 2d-*A* contains 27 atoms as shown in Fig. 3a, of which 13 atoms belong to the $Fe_2O(PO_4)_2$ framework and the remaining 14 atoms belong to the guest species. Both iron atoms bond with 5 oxygen atoms arranged in trigonal pyramids (4 O of PO_4 groups and one O atom shared between 3 Fe atoms) with an average Fe–O distance of 1.942 Å. The axial and equatorial O–Fe–O angles are provided in Table 4. Each P1 makes 4 P1–O–Fe linkages with P1–O bond lengths in the range of 1.529–1.547 Å and the O–P1–O bond angles in the range of 106.5–111.7°. However, each P2 makes only 3 P2–O–Fe linkages with the bond lengths in the range of 1.529–1.571 Å while terminal O–P2 distance is shorter 1.503(3) Å and the O–P2–O bond angles in the range of 107.3–111.7°. Bond valence sum calculation [38] clearly indicates that the valence status of the Fe and P are +3 and +5, respectively, which is in agreement with the framework formula. The structure of 2d-*A* consists of double sheet layers with enH_2^{2+} between them as shown in Fig. 3b. Four trigonal bipyramids form a block in which two trigonal bipyramids of Fe2 share an edge giving an Fe2–Fe2 distance of 2.895(1) Å. The other Fe1 pyramid shares one corner with the Fe2–Fe2 pair (Fig. 3c) resulting in 3.387(1) and 3.555(1) Å Fe1–Fe2 distances. The tetrameric block is centrosymmetric with the symmetry center lying in the middle of the shared edge. The PO_4 tetrahedra share corners and link the Fe atoms in and between the blocks forming the layer with $P2_1/c$ symmetry (Fig. 3d). The two Fe–O–P–O–Fe bridges between blocks are relatively short with Fe–Fe distances of 4.762(1) and 4.815(1) Å. P1 tetrahedron shares all four corner with two building blocks, and P2 tetrahedron shares only three corners with two blocks while the remaining corner is terminal and points outside the layer as shown in Fig. 3b. A single sheet of the layer can be shown as a net of eight- and four-membered rings of alternating trigonal bipyramids and tetrahedra. The amine molecules are located between the layers and form 9 N–H···O H-bonds with the phosphate groups. The N1 ammonium group forms five H-bonds binding the layers together. Interestingly, the N2 ammonium group is practically inside the layer (Fig. 3b) and forms four H-bonds within the layer. This structure is quite similar to the compound of the propylene diammonium compound $(NH_3CH_2CH_2CH_2NH_3)Fe_2O(PO_4)_2$ that has the same layers but slightly different packing due to the longer and different in shape intercalating molecule [19].

The structures of the 1d, 2d-*B*, lipscombite and 3d-Fe materials have been studied previously. We obtained similar results from a single crystal study as outlined in Table 6. The frameworks in the 1d, 2d-*B* and 3d-lipscombite structures are built from chains of Fe octahedra that share corners, edges and faces, respectively, as shown in Fig. 4. In the 1d compound, the corner-sharing iron octahedra are additionally linked along the chain by HPO_4 groups as shown in Fig. 4a. The shared corner is coordinated to a hydrogen atom to form a *trans*-hydroxyl group. This chain is similar to that found in $[(1R,2R)\text{–}C_6H_{10}(NH_2)_2][Ga(OH)$

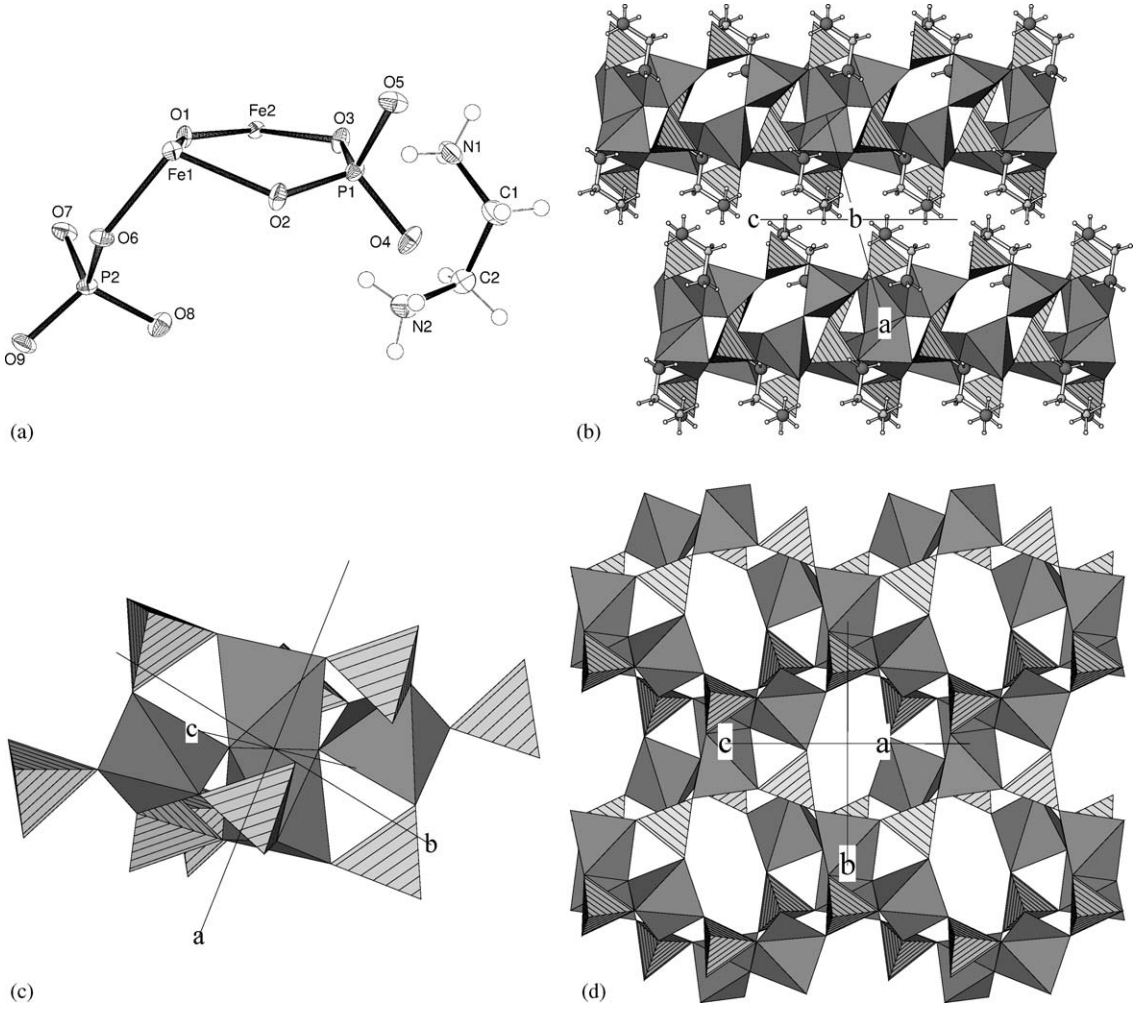

Fig. 3. Crystal structure of 2d-*A*. (a) Ortep view of 2d-*A* with thermal ellipsoids at 50%; (b) stacking of layers in 2d-*A* in projection along *Y*; shortest H-bonds (one for each H atom) are shown as thin lines; (c) the tetramer of Fe and phosphorous polyhedra; and (d) double sheet layer of 2d-*A* in projection on *YZ*; PO_4 tetrahedra are lined.

Table 6
Cell parameters of 1d, 2d-*B*, 3d-Fe

	1d our data	1d in Ref. [12]	2d-*B* in Ref. [16]	Lipscombite in Ref. [35]	3d-Fe our data	3d-Fe in Ref. [24]
Sp. gr.	$P\bar{1}$	$P\bar{1}$	$P2_1/c$	$P4_32_12$	$C2$	$C2$
a (Å)	8.541(1)	8.526(2)	4.5010(7)	7.310(3)	30.310(5)	30.3801(5)
b (Å)	9.798(1)	9.796(2)	6.114(1)	7.310(3)	10.095(2)	10.1204(5)
c (Å)	7.253(1)	7.232(2)	18.460(3)	13.212(7)	10.080(2)	10.0977(5)
α (deg)	90.580(2)	90.25(2)	90	90	90	90
β (deg)	92.356(2)	92.72(2)	94.59(1)	90	107.701(3)	107.712(1)
γ (deg)	65.610(2)	65.20(1)	90	90	90	90
R	0.048	0.040	0.049	0.102	0.089	0.049

$(HPO_4)_2] \cdot H_2O$ [39]. The Ga–O distances 1.967 Å and 2.007 Å are alternating along the chain, while the Fe–O distances are identical 1.986 Å. In the 2d-*B* compound, infinite chains of edge-sharing iron octahedra are linked into 2d layers through the phosphate tetrahedra. Similarly to the 1d material, the Fe octahedra have two OH groups opposite to each other, while the four other corners are occupied by four oxygen atoms from the phosphate groups. Meanwhile, one of the oxygen atoms in phosphate tetrahedra is not coordinated. In lipscombite, two perpendicular oriented face-sharing chains of iron octahedra are connected into a 3d framework by sharing corners with each other and with phosphate to form the ''rod-packing'' structure [40].

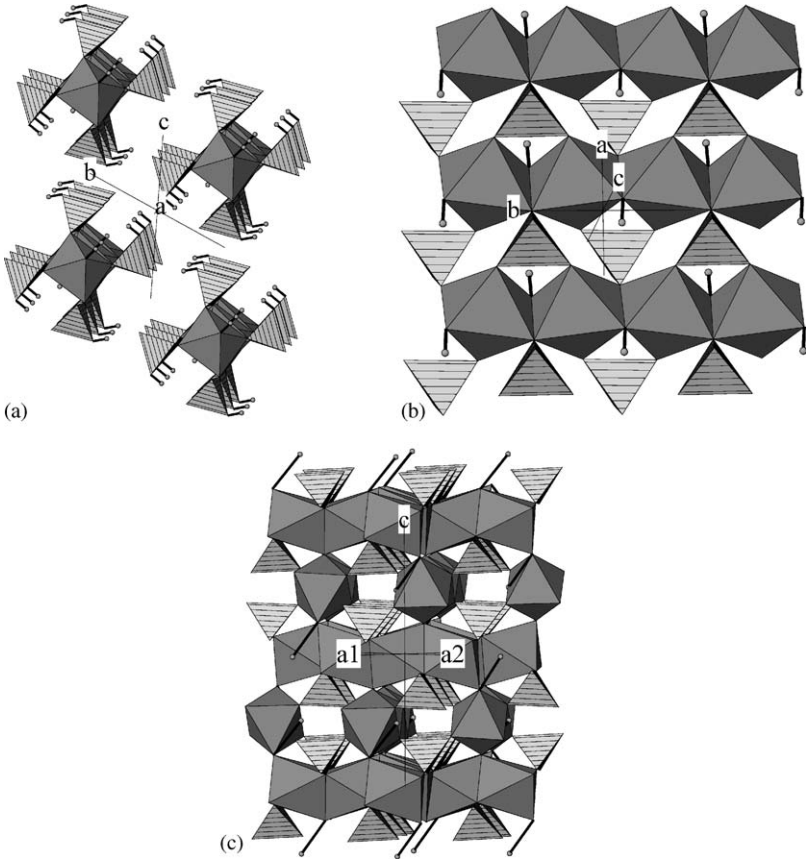

Fig. 4. Structures of (a) 1d, (b) 2d-*B* and (c) Lip. The PO_4 tetrahedra are lined. Small circles show H atoms from hydroxyl groups.

Similarly to the two other structures described above, the Fe octahedra consists of four oxygen atoms from PO_4 and two oxygen atoms of opposite OH groups. In this compound the phosphate group shares all four corners with iron octahedra. As mentioned before, the 1d compound can react with amine to form the 2d-*B* compound and at high temperatures it loses the organic and turns into lipscombite. It can be concluded that the iron phosphates with high dimensionality are built up from the lower dimensionality compound as proposed by Rao et al. [41] for zinc phosphate materials. Here, the 1d chain can be interconnected to form the layered and then the 3d structures. Since the Fe/P ratio increases in going from the 1d to the 3d compounds there is a greater degree of sharing of the polyhedra, so the iron octahedra go from corner-sharing to face-sharing.

In the 3d-Fe compound, the network is built from two kinds of alternating clusters, as shown in Fig. 5. In one cluster, all the four iron atoms are five-coordinated (trigonal bipyramid), while in the other only three Fe atoms are five-coordinated with the remained one six-coordinated (octahedra). This confirms the results of Huang et al. [24]. According to the bond valence sum calculations, half the Fe atoms in each cluster have oxidation state 3+ and the other half 2+. The manganese substitution is believed to take the ferrous position in the 3d-Fe compound giving Mn_2Fe_2 clusters. The powder X-ray pattern of the 3d-Mn compound is in good agreement with the calculated pattern for the compound; to date no satisfactory single crystal data has been obtained. Both the Fe and Mn_2Fe_2 structures are pseudo-tetragonal, e.g. the monoclinic cell of the Fe structure (space group C2) can be approximately transformed into tetragonal $I\overline{4}2m$ as $\mathbf{a}_I = \mathbf{c}_C$, $\mathbf{b}_I = \mathbf{b}_C$, $\mathbf{c}_I = (\mathbf{a}_C + \mathbf{c}_C)/3$. This causes multiple twinning on the micro level, which combined with a monoclinic unit cell just slightly different from tetragonal, makes it difficult to obtain satisfactory structural data.

3.3. Magnetic study

The temperature dependence of the magnetic susceptibility and FC/ZFC curves of 2d-*A* $(enH_2)Fe_2O(PO_4)$ are shown in Fig. 6a. Two distinct magnetic transitions are observed at about 160 and 30 K. Below 160 K, ZFC and FC data diverge, indicating the onset of irreversible magnetic behavior. The effective magnetic moment per iron ion, calculated from the χT value (Fig. 6b) is 3.20 μ_B ($T = 298$ K), i.e., significantly lower than 5.92 μ_B expected for Fe^{3+}, the magnetic moment further drops with decreasing temperature. This behavior indicates a short-range antiferromagnetic (AF) ordering of spins,

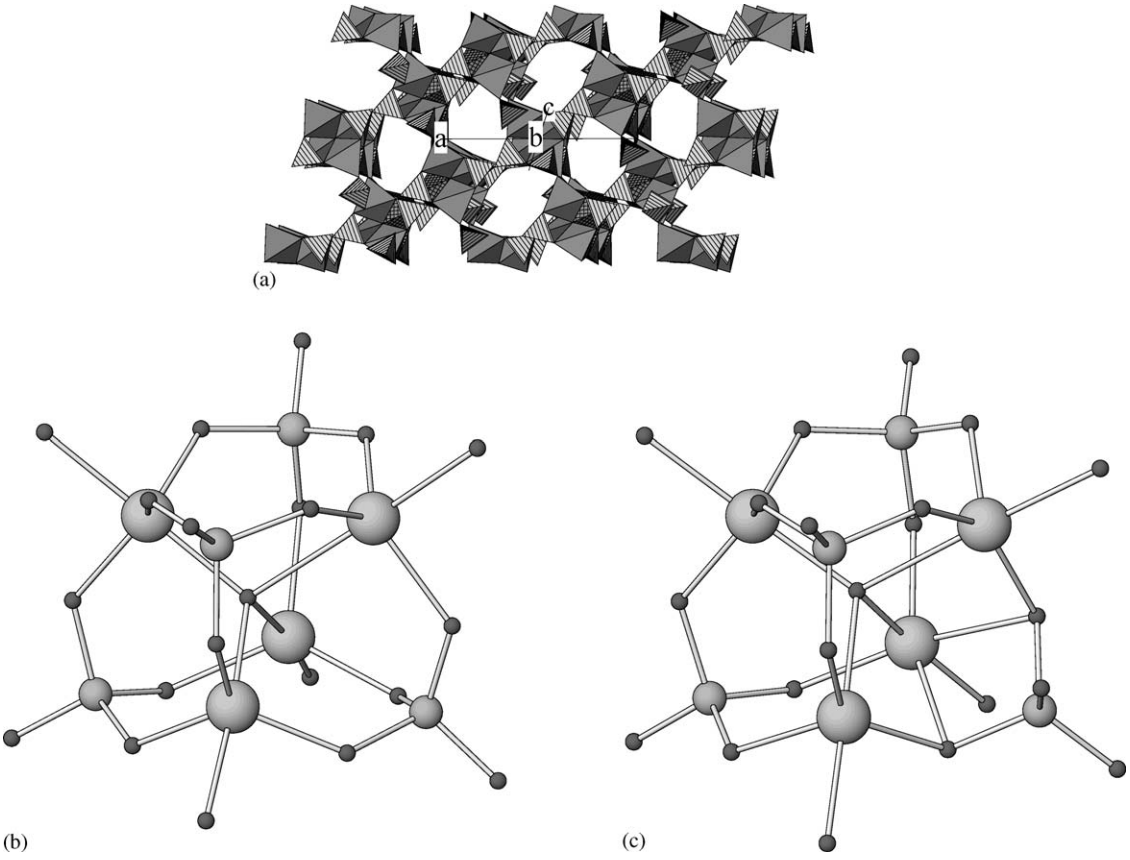

Fig. 5. Crystal structure of 3d-Fe (a) polyhedral view; PO_4 tetrahedra are lined; FeO_6 octahedra are gridded. (b) Cluster 1 with all FeO_5 trigonal bipyramids. (c) Cluster 2 with 3 FeO_5 trigonal bipyramids and one FeO_6 octahedra. Large circles depict iron, medium—phosphorous, small—oxygen.

which is in agreement with Goodenough's rules, predicting AF superexchange for d^5-d^5 interactions [42]. Short Fe–Fe distances in the cluster of four FeO_5 trigonal bipyramids may provide quite strong exchange, therefore the high-temperature transition could correspond to the magnetic ordering of these clusters. However, magnetic network of the cluster is geometrically frustrated: iron atoms form two triangular platelets sharing an edge, so that all AF interactions cannot be satisfied simultaneously [43]. An unusually strong AF exchange on geometrically frustrated lattice may lead to the high-temperature irreversible behavior observed. FeO_5 tetramers are connected in 2d network via PO_4 tetrahedra and are coupled magnetically by weak supersuperexchange interactions. Then, the long-range 2d or 3d order is established at significantly lower temperature of 30 K.

The magnetic properties of the compounds with somewhat similar structure have been reported elsewhere [19,43]. For propylene diammonium analog of our compound, which is also built of FeO_5 tetramers, the value of magnetic moment per iron atom is 2.58 μ_B at 300 K and decreases with temperature. The low value of the magnetic moment is in qualitative agreement with our data, however, no magnetic transitions were reported for that compound [19]. Spheniscidite $NH_4[Fe_2(OH)(PO_4)_2]\cdot H_2O$, the 3d compound built of similar tetramer of FeO_6 octahedra, orders antiferromagnetically at $T_N = 10$ K, while the asymptotic Curie–Weiss temperature was found $\Theta_p = -300$ K. Very large $|\Theta_p/T_N| = 30$ ratio is consistent with the presence of magnetic frustration [43]. Thus, the two magnetic transitions and the high-temperature irreversible magnetic behavior observed in $(enH_2)Fe_2O(PO_4)$ are new and very interesting phenomena. We are working toward clarifying their nature.

The magnetic properties of other compounds presented in this paper are better understood. The temperature dependence of magnetic susceptibility for the 1d $(enH_2)Fe(HPO_4)_2(OH)\cdot H_2O$ (Fig. 7) exhibits characteristic broad maximum at about 130 K, indicating 1d AF ordering along chains of corner-sharing FeO_6 octaherda. From the temperature of the $\chi(T)$ maximum, the exchange constant can be estimated as $|J|/k \approx 12$ K using the relation for spin 5/2 Heisenberg chain: $kT(\chi_{max})/|J| \approx 10.6$ [44]. The Curie-like growth and further drop of the susceptibility observed at low temperature could be due to paramagnetic impurities

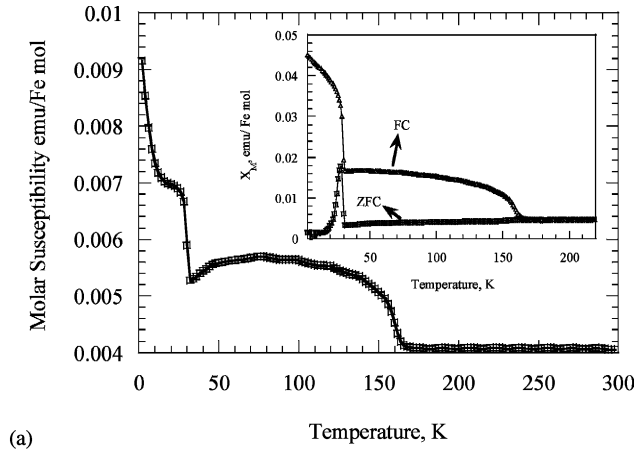

(a)

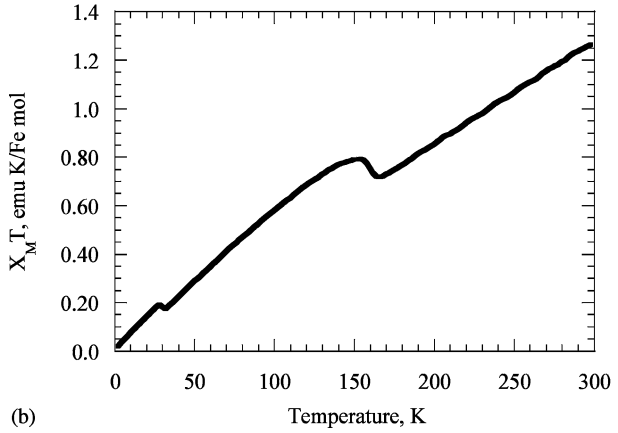

(b)

Fig. 6. Temperature dependence of magnetic susceptibility for 2d-*A*; inset shows FC and ZFC susceptibilities. (b) Temperature dependence of χT for 2d-*A*.

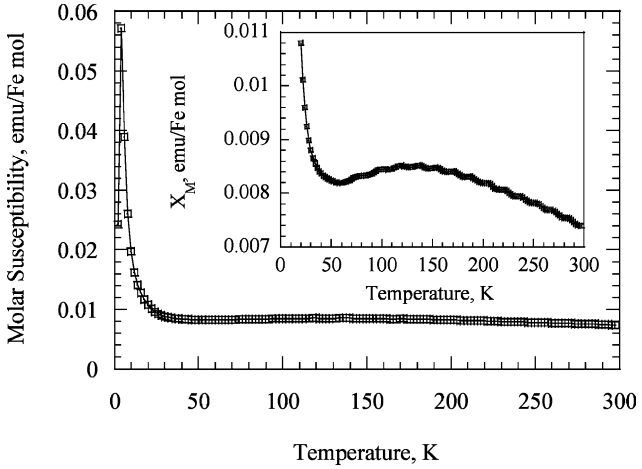

Fig. 7. Temperature dependence of magnetic susceptibility for 1d; inset magnifies the high-temperature region.

undergoing ordering transition at 3.9 K. The 1d ordering in a chain of corner-sharing FeO_6 octahedra was observed earlier in synthetic tavorite $LiFe(PO_4)(OH,F)$, with exchange constant also about 12 K [45].

The magnetic susceptibility of the 2d-*B* $(enH_2)Fe_2(PO_4)_2(OH)_2$ follows the Curie–Weiss law at temperatures above 50 K (Fig. 8). The asymptotic Curie–Weiss temperature of $\Theta_p = -100$ K indicates strong AF interactions between the iron spins. At $T = T_N = 30$ K the AF ordering transition is observed. At the same temperature FC and ZFC data becomes different, indicating a spin-glass-like transition. The value of ratio $|\Theta_p/T_N| = 3.33$ exceeds unity, confirming the presence of magnetic frustrations. The nature of the ordered magnetic state in this compound was studied by Debord and co-authors [16]. They observed a non-zero net magnetic moment in both ac susceptibility and dc magnetization data and proposed canted AF or weak ferromagnetic order. The exact nature of the ordered state and the origin of magnetic frustration in this compound still remains unclear, and we are placing

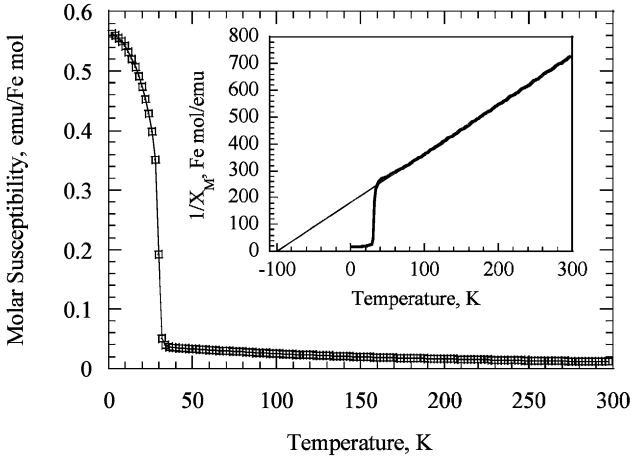

Fig. 8. Temperature dependence of magnetic susceptibility for 2d-*B*; inset shows the thermal evolution of inverse molar susceptibility corrected due to core diamagnetism.

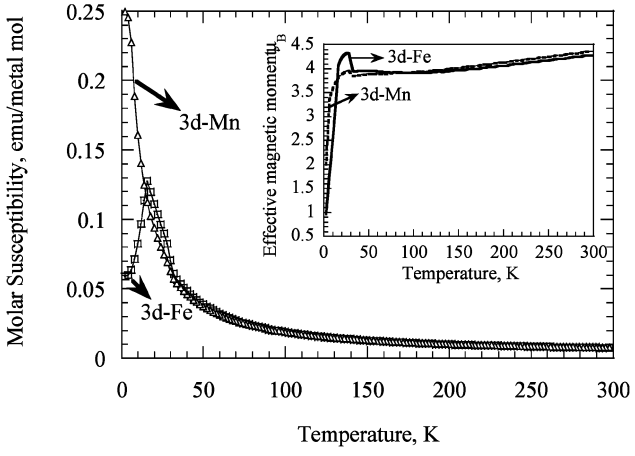

Fig. 9. Temperature dependence of magnetic susceptibility for the 3d-Fe and 3d-Mn compounds; inset shows temperature dependence of effective magnetic moment.

additional experimental and theoretical efforts toward studying these phenomena.

A pronounced magnetic transition at 27 K was observed for the 3d-Fe $(enH_2)_2Fe_4O(PO_4)_2 \cdot H_2O$ while no ordering was found in its Mn-substituted analog over the investigated temperature range (Fig. 9). Above 27 K, the susceptibility data follows the Curie–Weiss law; the effective magnetic moment per iron or manganese atom is about 4 μ_B up to 150 K, increasing to 4.23 μ_B at room temperature. The nature of the ordered state in 3d-Fe and the depression of the magnetic transition temperature in Mn-3d is a subject of our future research.

Acknowledgments

The support of this work by the National Science Foundation, DMR 9810198, is greatly appreciated.

References

[1] G. Ferey, A.K. Cheetham, Science 283 (1999) 125.
[2] P.B. Moore, Am. Mineral. 55 (1970) 135.
[3] Y. Song, P.Y. Zavalij, M. Suzuki, M.S. Whittingham, Inorg. Chem. 41 (2002) 5778.
[4] L. Mundi, R.C. Haushalter, Inorg. Chem. 31 (1992) 3050.
[5] P. Lightfoot, D. Masson, Mater. Res. Bull. 30 (1995) 1005.
[6] S.S. Dhingra, R.C. Haushalter, J. Chem. Soc. Chem. Commun. 21 (1993) 1665.
[7] V. Soghomonian, Q. Chen, R.C. Haushalter, J. Zubieta, C.J. O'Connor, Science 259 (1993) 1596.
[8] M. Cavellec, D. Riou, J.M. Greneche, G. Ferey, Inorg. Chem. 36 (1997) 2187.
[9] H.M. Lin, K.H. Lii, Inorg. Chem. 37 (1998) 4220.
[10] S. Mahesh, M.A. Green, S. Natarajan, J. Solid State Chem. 165 (2002) 334.
[11] V. Zima, K.H. Lii, J. Chem. Soc. Dalton Trans. (1998) 4109.
[12] Z.A.D. Lethbridge, P. Lightfoot, R.E. Morris, D.S. Wragg, P.A. Wright, J. Solid State Chem. 142 (1999) 455.
[13] M.R. Cavellec, D. Riou, G. Ferey, Acta Crystallogr. C 51 (1995) 2242.
[14] A. Choudhury, S. Natarajan, C.N.R. Rao, J. Chem. Soc. Chem. Commun. (1999) 1305.
[15] M.R. Cavallec, J.M. Greneche, D. Riou, G. Ferey, Chem. Mater. 10 (1998) 2434.
[16] J.R.D. Debord, W.M. Reiff, R.C. Haushalter, J. Zubeta, J. Solid State Chem. 125 (1996) 186.
[17] M.R. Cavellec, G. Ferey, J.M. Greneche, J. Magn. Magn. Mater. 174 (1997) 109.
[18] K.H. Lii, Y.F. Huang, J. Chem. Soc. Chem. Commun. (1997) 2221.
[19] K.H. Lii, Y.F. Huang, J. Chem. Soc. Chem. Commun. (1997) 1311.
[20] J.R.D. Debord, W.M. Reiff, C.J. Warren, R.C. Haushalter, J. Zubieta, Chem. Mater. 9 (1997) 1994.
[21] A. Choudhury, S. Natarajan, Int. J. Inorg. Mater. 2 (2000) 217.
[22] A. Choudhury, S. Natarajan, J. Solid State Chem. 154 (2000) 507.
[23] K.H. Lii, Y.F. Huang, J. Chem. Soc. Chem. Commun. (1997) 839.
[24] C.Y. Huang, S.L. Wang, K.H. Lii, J. Porous Mater. 5 (1998) 147.
[25] M. Cavellec, D. Riou, J.-M. Greneche, G. Ferey, J. Magn. Magn. Mater. 163 (1996) 173.
[26] K.-W. Lii, Y.-F. Huang, V. Zima, C.-Y. Huang, H.-M. Lin, Y.-C. Jiang, F.-L. Liao, S.-L. Wang, Chem. Mater. 10 (1998) 2599.
[27] A. Muller, H. Reuter, S. Dillinger, Angew. Chem. Int. Ed. Engl. 34 (1995) 2328.
[28] R.J. Francis, S. O'Brien, A.M. Fogg, P.S. Halasyamani, D. O'Hare, T. Loiseau, G. Ferey, J. Am. Chem. Soc. 121 (1999) 1002.
[29] R.I. Walton, T. Loiseau, D. O'Hare, G. Ferey, Chem. Mater. 11 (1999) 3201.
[30] F. Taulelle, M. Haouas, C. Gerardin, C. Estournes, T. Loiseau, G. Ferey, Colloids Surf. A 158 (1999) 299.
[31] R.I. Walton, A.J. Norquist, S. Neeraj, S. Natarajan, C.N.R. Rao, D. O'Hare, J. Chem. Soc. Chem. Commun. (2001) 1990.
[32] A.A. Ayi, A. Choudhury, S. Natarajan, S. Neeraj, C.N.R. Rao, J. Mater. Chem. 11 (2001) 1181.
[33] A. Choudhury, S. Natarajan, S. Neeraj, C.N.R. Rao, J. Mater. Chem. 11 (2001) 1537.
[34] A. Choudhury, S. Neeraj, S. Natarajan, C.N.R. Rao, J. Mater. Chem. 12 (2002) 1044.
[35] I. Vencato, E. Mattievich, Y.R. Mascarenhas, Am. Miner. 74 (1989) 456.
[36] G.M. Sheldrick, SHELXL-97, University of Göttingen, Germany, 1997.
[37] N. Rajic, R. Gabrovsek, V. Kaucic, Thermochim. Acta 359 (2000) 119.
[38] I.D. Brown, D. Altermatt, Acta Crystallogr. B 41 (1985) 244.
[39] H.M. Lin, K.H. Lii, Inorg. Chem. 37 (1998) 4220.
[40] M. Keefee, S. Andersson, Acta Crystallogr. A 33 (1977) 914.
[41] C.N. Rao, S. Natarajan, A. Choudhury, S. Neeraj, A.A. Ayi, Acc. Chem. Res. 34 (2001) 80.
[42] J.B. Goodenough, Magnetism and the Chemical Bond, Interscience, New York, 1963.
[43] M. Cavellec, G. Ferey, J.M. Greneche, J. Magn. Magn. Mater. 167 (1997) 57.
[44] R. Carlin, Magnetochemistry, Springer, Berlin, 1986.
[45] J.L. Pizarro-Sanz, J.M. Dance, G. Villeneuve, M.I. Arriortua-Marcaida, Mater. Lett. 18 (1994) 327.